

Classical bridge functions in classical and quantum plasma liquids

F. Lucco Castello¹, P. Tolias¹ and T. Dornheim^{2,3}

¹ *Space and Plasma Physics - Royal Institute of Technology (KTH), SE-10044 Stockholm, Sweden*

² *Center for Advanced Systems Understanding (CASUS), D-02826 Görlitz, Germany*

³ *Helmholtz-Zentrum Dresden-Rossendorf (HZDR), D-01328 Dresden, Germany*

Bridge functions, the missing link in the exact description of strong correlations, are indirectly extracted from specially designed molecular dynamics simulations of classical one-component plasma liquids and accurately parameterized. Their incorporation into an advanced integral equation theory description of Yukawa one-component plasma liquids and a novel dielectric formalism scheme for quantum one-component plasma liquids leads to an unprecedented agreement with available molecular dynamics simulations and new *ab initio* path integral Monte Carlo simulations, respectively.

Strongly coupled charged systems, naturally occurring or engineered, are ubiquitous in disparate environments from high-energy-density [1, 2] to soft matter [3, 4]. They consist of classical point particles or fermions interacting via bare or screened Coulomb pair potentials [5]. Central to their understanding are three idealized models, whose analysis has led to key physical insights, namely the classical or quantum one-component plasma (OCP) [6–8] and classical Yukawa one-component plasma (YOCP) [9, 10]. The OCP and the YOCP liquid states, although squeezed in a rather small portion of the phase diagram between the gas and the crystal states, have proven to be the most theoretically elusive due to their lack of small parameters that forbid perturbative expansions viable for weak interactions or small vibrations [11, 12]. A particular attention has been paid to their structural and thermodynamic properties, since these also constitute input for advanced theoretical descriptions of collective modes [13–15], dynamical properties [16] and transport coefficients [17].

In the classical case, the integral equation theory (IET) of liquids constitutes the most accurate alternative to computer simulations for the determination of static pair correlations [18]. For one-component systems, it features two formally exact equations: the Ornstein-Zernike (OZ) integral equation and the non-linear equation [19, 20]

$$h(r) = c(r) + n \int c(r') h(|\mathbf{r} - \mathbf{r}'|) d^3r', \quad (1)$$

$$g(r) = \exp[-\beta u(r) + h(r) - c(r) + B(r)], \quad (2)$$

with $g(r)$ the radial distribution function (RDF), $h(r) = g(r) - 1$ the total correlation function (TCF), $c(r)$ the direct correlation function (DCF), $B(r)$ the bridge function [19]. A $B[h]$ functional relation is required in order to close the system. In diagrammatic analysis, the bridge function is represented by densely connected irreducible graphs and formally defined by virial-type series that involve Mayer functions or TCFs [21]. Both series converge very slowly and their high-order terms promptly become too complicated to calculate [22]. Furthermore, as pure diagrammatic objects, bridge functions lack a probabilistic interpretation and cannot be expressed as ensemble averages of functions that depend on instantaneous particle configurations, implying that they can only be indirectly extracted from simulations; a notoriously difficult

task [23–26]. Thus, numerous IET approaches have been developed that approximate the bridge function with a varying complexity [27], the simplest being the hypernetted chain (HNC) approach that drops it altogether [19].

Here, we extract the classical OCP bridge functions at multiple states, spanning the dense liquid region, from specially designed molecular dynamics (MD) simulations and construct an analytic parametrization. This is incorporated into the recent isomorph-based empirically modified hypernetted chain approach (IEMHNC) based on the excess entropy invariance of YOCP bridge functions [28] and into a novel dielectric quantum OCP scheme based on the exact classical-limit correlations. Theoretical predictions are compared with available MD and new path integral Monte Carlo (PIMC) simulations, respectively.

Classical OCP bridge function extraction. The classical OCP concerns point charges that are immersed in a rigid neutralizing background. The thermodynamic states are fully specified by one dimensionless quantity [6]: the coupling parameter $\Gamma = \beta Q^2/d$ where $d = [4\pi n/3]^{-1/3}$ is the Wigner-Seitz radius and $\beta = 1/(k_B T)$. We focus on moderate densities above the Kirkwood point $\Gamma_K \simeq 1.12$ [29] and prior to the bcc crystallization point $\Gamma_m \simeq 171.8$ [30]. Bridge functions will be extracted for 18 state points, $\Gamma = 10, 20, \dots, 170$. The methodology developed in Ref. [26] needs to be modified for the OCP due to the long-range Coulomb interactions. In what follows, we briefly present these peculiarities. Reduced $x = r/d$ units are employed.

Outside the correlation void where $g(x) \simeq 0$ ($x > 1.2$), bridge functions are indirectly extracted with the *OZ inversion method* [26, 31]. NVT MD simulations are carried out with $N = 54872$ particles, 2^{20} equilibration time-steps and 2^{23} time-steps for statistics. The long-range interactions are handled with the Ewald sum implemented with the particle-particle particle-mesh (PPPM) technique [32]. The RDF is extracted from histograms with a $\Delta x = 0.002$ bin width. The Lebowitz-Percus size correction is applied, $g(x) = g_{MD}(x)(1 + \chi_T/N)$ [33], with χ_T the reduced isothermal compressibility from the hyper-virial route. FFT is used to compute the static structure factor $S(k)$ and Padé approximants are utilized to ensure that the compressibility sum rule is exactly satisfied [6]. Inverse FFT with long-range decomposition is employed to determine the DCF from the Fourier transformed OZ.

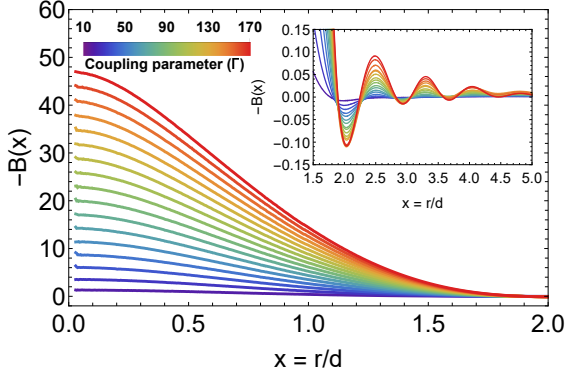


FIG. 1: Results for 18 OCP states. Extracted bridge functions in their monotonic (main) and oscillatory decay range (inset).

TABLE I: Fit parameters for the analytic parametrization of the short and intermediate range bridge function in Eq.(3).

	$j = 0$	$j = 1$	$j = 2$	$j = 3$	$j = 4$
s_0^j	0.076912	-0.10465	0.0056629	0.00025656	N/A
s_2^j	0.068045	-0.036952	0.048818	-0.0048985	N/A
s_3^j	-0.30231	0.30457	-0.11424	0.0095993	N/A
s_4^j	0.25111	-0.26800	0.082268	-0.0064960	N/A
s_5^j	-0.061894	0.066811	-0.019140	0.0014743	N/A
l_0^j	0.25264	-0.31615	0.13135	-0.023044	0.0014666
l_1^j	-12.665	20.802	-9.6296	1.7889	-0.11810
l_2^j	15.285	-14.076	5.7558	-1.0188	0.06551
l_3^j	35.330	-40.727	16.690	-2.8905	0.18243

Eq.(2) can now be solved for the bridge function.

Within the correlation void ($x < 1.4$), bridge functions are indirectly extracted with the *cavity method* [26, 34]. NVT MD simulations are performed featuring two tagged particles whose artificial pair interactions $\psi(x) = \chi(x) + \phi(x)$ enable sampling of the cavity distribution function (CDF) $y_{\text{sim}}(x) = g^{12}(x) \exp[\beta\psi(x)]$. In order to enhance sampling, the correlation void is split into four successive overlapping windows by imposing hard constraints in the tagged pair motion through the $\chi(x)$ component that realizes a smooth potential well. Aiming to achieve uniform sampling, multiple small simulations are run to optimize the $\phi(x)$ component that is determined by supplementing the prescription of Ogata [35] with a linear adder. NVT MD simulations are performed with $N = 1000$ particles (useful statistics from the tagged pair), 2^{20} equilibration time-steps and $2^{31} - 2^{32}$ time-steps for statistics. The CDFs of the real and simulated system are connected by $y(x) = Cy_{\text{sim}}(x) \exp[(\Gamma/x)\text{erf}(a_s x)]$ with a_s the Ewald splitting parameter and the constant C determined from CDF continuity within the entire range. Eq.(2) can now be re-written via $y(r)$ and solved for the bridge function.

Extraction uncertainties stem exclusively from statistical errors due to the finite simulation duration, since tail errors are negligible, finite-size errors are corrected and grid errors are minimized [26]. All extracted OCP bridge

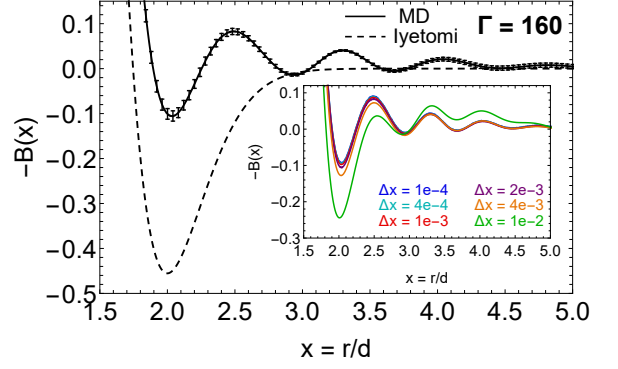


FIG. 2: Results for $\Gamma = 160$. Our extracted $B(r)$ with the estimated total uncertainties vs the Iyetomi $B(r)$ within the oscillatory decay range (main). Our extracted $B(r)$ for varying histogram bin widths: $\Delta x \lesssim 0.003$ leads to indistinguishable $B(r)$, whereas $\Delta x \gtrsim 0.01$ leads to large grid errors (inset).

functions are featured in Fig.1 for their non-trivial range.

Classical OCP bridge function parametrization. A simple strategy was developed to obtain an analytic expression. First, the monotonic short range of the bridge function is fitted with a fifth order polynomial without a linear term, as suggested by Widom's theorem [36] and the soft mean spherical approximation [37]. Then, the oscillatory decaying intermediate range of the bridge function is fitted with a combination of exponents and cosines. Finally, exploiting the overlap of the two ranges, the transition is well-described with a sigmoid switching function:

$$B_{\text{OCP}}(x, \Gamma) = [1 - f(x)] B_S(x, \Gamma) + f(x) B_I(x, \Gamma), \quad (3)$$

$$B_S(x, \Gamma) = s_0(\Gamma) + \sum_{i=2}^5 s_i(\Gamma) x^i,$$

$$B_I(x, \Gamma) = l_0(\Gamma) \Gamma^{5/6} \exp[-l_1(\Gamma)(x - 1.44) - 0.3x^2] \times \\ \{\cos[l_2(\Gamma)(x - 1.44)] + l_3(\Gamma) \exp[-3.5(x - 1.44)]\}, \\ f(x) = 0.5 \{1 + \text{erf}[5.0(x - 1.5)]\},$$

and $s_i(\Gamma) = \sum_{j=0}^3 s_i^j \Gamma (\ln \Gamma)^j$, $l_i(\Gamma) = \sum_{j=0}^4 l_i^j \Gamma^{1/6} (\ln \Gamma)^j$ being monotonic functions of Γ . The s_i^j, l_i^j coefficients are listed in Table I. For all states, the fit is near-exact within $0 \leq x \leq 3$ but it fails to describe higher order damped oscillations that arise up to $x \simeq 5$ near the melting point.

OCP bridge functions were earlier extracted and parameterized by Iyetomi and coworkers [38] whose procedure has numerous deficiencies: (a) The short range was determined with extrapolations based on Widom's theorem [36] and on Jancovici's exact result [39]. (b) The RDF histograms had a relatively large bin width of $\Delta x = 0.04$ leading to large local grid errors. (c) The extraction concerned only 4 state points. (d) The parametrization consisted of a high-order polynomial multiplied by an exponentially decaying function, leading to a single extremum curve. Although the extrapolation method turned out to be quite accurate, the other deficiencies are impactful. In particular, the large grid errors are revealed in Fig.2.

Application to classical plasma liquids. The classical YOCP concerns point charges embedded in a polarizable

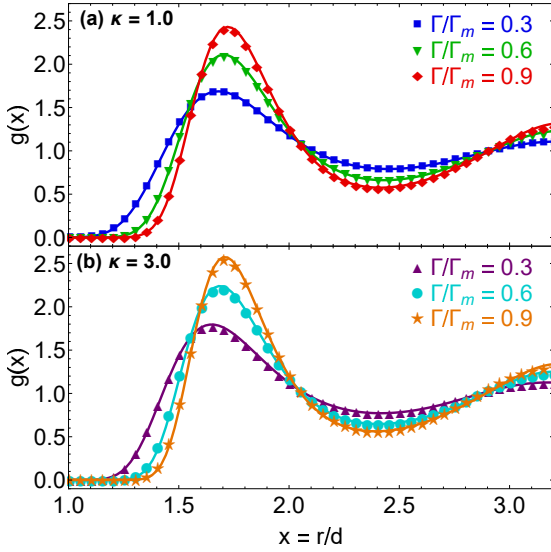


FIG. 3: Radial distribution functions resulting from MD simulations (discrete points) and the updated IEMHNC approach (solid lines): (a) $\kappa = 1$ and $\Gamma/\Gamma_m = 0.3$ (blue), 0.6 (green), 0.9 (red) with $\Gamma_m = 220.18$, (b) $\kappa = 3$ and $\Gamma/\Gamma_m = 0.3$ (purple), 0.6 (cyan), 0.9 (orange) with $\Gamma_m = 1234.51$.

neutralizing background. The thermodynamic states are fully specified by two dimensionless quantities [9, 40]: the coupling parameter Γ and screening parameter $\kappa = d/\lambda_s$ with λ_s a shielding length. The OCP is recovered as $\kappa \rightarrow 0$. We focus on moderate densities above the Kirkwood line [29] and prior to the bcc/fcc crystallization [30].

It has recently been demonstrated that the YOCP exhibits very strong correlations between its virial and potential energy constant volume thermal equilibrium fluctuations [41]. Thus, the YOCP belongs to the class of R-simple systems and possesses isomorph lines, *i.e.* phase diagram curves of constant excess entropy along which a set of structural and dynamic properties are nearly invariant when expressed in properly reduced units [42, 43]. In particular, the isomorph lines are nearly parallel to the melting line [44] and accurately parameterized by [41, 45]

$$\Gamma_{\text{ISO}}(\Gamma, \kappa) = \Gamma e^{-\alpha\kappa} [1 + \alpha\kappa + (1/2)(\alpha\kappa)^2] = \text{const.} \quad (4)$$

with $\alpha = n^{-1/3}/d = (4\pi/3)^{1/3}$. Our recent YOCP simulations confirmed our conjecture [28] that the reduced-unit bridge functions of R-simple systems are isomorph invariant [26]. Thus, given the Eq.(5) mapping of configurational adiabats, OCP bridge functions constitute the basis for the construction of YOCP bridge functions via

$$B_{\text{YOCP}}(x, \Gamma, \kappa) = B_{\text{OCP}}[x, \Gamma_{\text{ISO}}(\Gamma, \kappa)]. \quad (5)$$

This IET closure amounts to the IEMHNC approach that was earlier combined with the Iyetomi OCP bridge function and applied to the YOCP [28]. It was revealed that this early IEMHNC version could reproduce the YOCP thermodynamic properties within 0.5% and the YOCP structural properties within 1.5% in the first coordination

TABLE II: Interaction energy $\tilde{u} = (\pi\lambda r_s)^{-1} \int_0^\infty [S(x) - 1] dx$ (in Hartree units) of the unpolarized electron liquid: finite-size corrected PIMC, HNC-STLS and IET-STLS results. The PIMC data for the first six states are adopted from Ref.[61], whereas the PIMC data for the remaining 14 states are new.

r_s	θ	\tilde{u} PIMC	\tilde{u} HNC-STLS	e_{HNC} (%)	\tilde{u} IET-STLS	e_{IET} (%)
100	0.50	-0.00825500	-0.00815866	1.167	-0.00822181	0.402
100	0.75	-0.00824570	-0.00816490	0.980	-0.00822544	0.246
100	1.00	-0.00823490	-0.00816618	0.834	-0.00822559	0.113
100	2.00	-0.00817650	-0.00812905	0.580	-0.00819066	0.173
100	4.00	-0.00800623	-0.00796833	0.473	-0.00803143	0.315
50	0.50	-0.01600700	-0.01589841	0.678	-0.01603510	0.176
60	0.50	-0.01345310	-0.01334804	0.781	-0.01346014	0.052
70	0.50	-0.01161175	-0.01150938	0.882	-0.01160390	0.068
80	0.50	-0.01021937	-0.01012012	0.971	-0.01020149	0.175
90	0.50	-0.00912862	-0.00903293	1.048	-0.00910415	0.268
110	0.50	-0.00752642	-0.00744012	1.147	-0.00749675	0.394
125	0.50	-0.00665421	-0.00657377	1.209	-0.00662268	0.474
125	0.75	-0.00665053	-0.00657838	1.085	-0.00662556	0.442
125	1.00	-0.00664336	-0.00657999	0.954	-0.00662647	0.254
125	1.50	-0.00662535	-0.00657432	0.770	-0.00662112	0.064
125	2.00	-0.00660298	-0.00655900	0.666	-0.00660712	0.063
150	0.50	-0.00558177	-0.00550821	1.318	-0.00554797	0.606
150	1.00	-0.00557134	-0.00551337	1.040	-0.00555132	0.359
200	0.50	-0.00422244	-0.00416445	1.373	-0.00419373	0.680
200	1.00	-0.00421710	-0.00416813	1.161	-0.00419559	0.510

cell [46]; an excellent performance comparable to that of the variational modified hypernetted chain approach [47] (VMHNC) that is 10–100 \times more computationally costly.

The updated IEMHNC approach is obtained by combining Eqs.(1,2) with Eqs.(3,4,5). This set is solved with Picard iterations in Fourier space combined with mixing and long-range decomposition techniques (when $\kappa < 1$). A comparison with extended simulation results from the literature [30, 48, 49] reveals that this IEMHNC version reproduces YOCP thermodynamic and structural properties within 0.5% in the dense liquid region; an unprecedented accuracy on par with that of modern simulations. This is highlighted in the graphical comparison between IEMHNC- & MD-generated RDFs featured in Fig.3.

Application to quantum plasma liquids. The quantum OCP concerns electrons immersed in a rigid ionic neutralizing background. In the unpolarized case of equal spin-up & -down electrons, thermodynamic states are specified by two dimensionless quantities [50]: the Brueckner parameter $r_s = d/a_B$ with $a_B = \hbar^2/(m_e e^2)$ the first Bohr radius and the degeneracy parameter $\theta = k_B T/E_F$ with $E_F = [(3\pi^2 n)^{2/3}/2](\hbar^2/m_e)$ the Fermi energy w.r.t spin-up electrons. We focus on high degeneracy ($\theta \sim 1$) moderate density ($r_s \gtrsim 10$) beyond warm dense matter [51] but prior to Wigner crystallization [52, 53], where correlations are strong but quantum effects remain important.

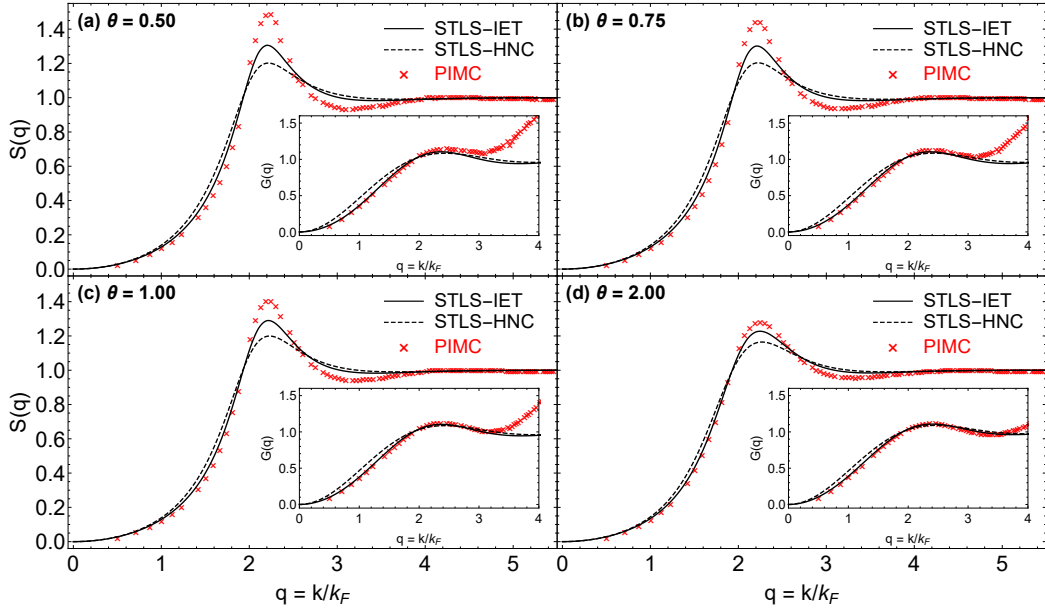


FIG. 4: Static structure factors (main) and static local field corrections (inset) resulting from PIMC simulations (red crosses), the HNC-STLS scheme (dashed black lines) and the IET-STLS scheme (solid black lines). Results for $r_s = 100$ and $\theta = 0.5, 0.75, 1, 2$.

In linear response theory, the exact density-density response function $\chi(\mathbf{k}, \omega)$ can always be expressed in terms of the ideal (Lindhard) density response $\chi_0(\mathbf{k}, \omega)$ and the unknown dynamic local field correction $G(\mathbf{k}, \omega)$ (LFC)

$$\chi(\mathbf{k}, \omega) = \frac{\chi_0(\mathbf{k}, \omega)}{1 - U(\mathbf{k}) [1 - G(\mathbf{k}, \omega)] \chi_0(\mathbf{k}, \omega)}, \quad (6)$$

with $U(\mathbf{k}) = 4\pi e^2/k^2$ the regularized Fourier transform of the Coulomb pair potential [54]. In addition, frequency integration of the quantum fluctuation-dissipation theorem (FDT) and analytic continuation of $\chi(\mathbf{k}, \omega)$ to the complex plane lead to a static structure factor $S(\mathbf{k})$ (SSF) relation that involves the Matsubara summation

$$S(\mathbf{k}) = -\frac{1}{n\beta} \sum_{l=-\infty}^{\infty} \tilde{\chi}(\mathbf{k}, i\omega_l), \quad (7)$$

with $\tilde{\chi}(\mathbf{k}, z)$ the complex-valued density-density response function, $\omega_l = 2\pi l/(\beta\hbar)$ the Matsubara frequencies [55]. Dielectric schemes approximate the LFC as a SSF functional $G \equiv G[S]$, leading to self-consistent approaches [8, 54]. Rigorous schemes that include quantum effects on the random phase approximation level and treat correlation effects classically (such as the STLS scheme [56, 57]) as well as semi-empirical schemes that utilize asymptotic limits and embody exact simulation results (such as the effective static approximation [58, 59]), approximate the LFC by a frequency-independent value, $G(\mathbf{k}, \omega) \equiv G(\mathbf{k})$.

A recently proposed scheme is singled out that belongs to the first group and treats strong correlations within the classical HNC approach [60, 61]. This HNC-STLS scheme combines the classical FDT, OZ equation and HNC non-linear equation to generate a frequency averaged $G[S]$

functional. Systematic comparison with PIMC results for moderate [60] and strong coupling [61] has revealed that the HNC-STLS is superior to other STLS-like schemes. To be specific, when $r_s \in [20, 100] \cap \theta \in [0.5, 4]$, its interaction energy predictions are accurate within 1.2% due to favorable error cancellations in the SSF integration [61] while its structural predictions are quite accurate for the SSF/LFC peak positions but significantly underestimate the SSF/LFC peak heights [61]. Considering that such a deficiency is also characteristic of the fully classical HNC approach [62, 63], it is expected that incorporation of the bridge function will lead to significant improvements. To this end, we generalize the HNC-STLS to a novel IET-STLS scheme by including our classical OCP bridge function. The $G[S]$ functional reads as

$$G(\mathbf{k}) = \frac{B(\mathbf{k})}{\beta U(\mathbf{k})} - \frac{1}{n} \int \frac{d^3 q}{(2\pi)^3} \frac{\mathbf{k} \cdot \mathbf{q}}{q^2} [S(|\mathbf{k} - \mathbf{q}|) - 1] \\ \times \left\{ -\frac{B(\mathbf{q})}{\beta U(\mathbf{q})} + 1 - [G(\mathbf{q}) - 1] [S(\mathbf{q}) - 1] \right\}, \quad (8)$$

and collapses to the HNC-STLS functional for $B(r) \equiv 0$. Use of the classical OCP bridge function necessitates the mapping of the quantum states (r_s, θ) to classical states (Γ) via $\Gamma = 2\lambda^2(r_s/\theta)$ with $\lambda^3 = 4/(9\pi)$. The Eqs.(6,7,8) form a closed set that is solved numerically. The computational cost drastically decreases by converting the triple to a double integral in Eq.(8) with two-center bipolar coordinates [37]. Faster Matsubara summation convergence is achieved by isolating the Hartree-Fock SSF in Eqs.(6,7) and faster high- k convergence for the double integral is achieved by isolating the STLS LFC in Eq.(8).

Aiming to validate the IET-STLS scheme against exact results, new PIMC simulations have been performed with

$N = 100$ electrons for 16 state points ($50 \leq r_s \leq 200$, $0.5 \leq \theta \leq 2.0$). In this phase diagram region, the fermion sign problem is weak due to the prevalence of strong correlations and the standard PIMC method suffices to obtain accurate results [8, 64]. Interaction energy finite-size errors stem from the omission of the long-wavelength contribution in the discretized version of the integral and are corrected applying the perfect screening sum rule [8, 61].

In terms of structure, our comparison reveals that: (a) the IET-STLS substantially improves the SSF peak magnitude and marginally improves the SSF peak position predictions of the HNC-STLS, (b) IET-STLS predictions for the static LFC are remarkably accurate especially for $k/k_F \leq 2$ with $k_F = (3\pi^2 n)^{1/3}$ the Fermi wavevector, (c) the IET-STLS drastically improves the static density-density response $\chi(\mathbf{k}, 0)$ predictions of the HNC-STLS. The conclusions are valid for all simulated state points, see Fig. 4 for typical examples. In terms of thermodynamics, the favorable error cancellation persists and, thus, the IET-STLS interaction energies are accurate within 0.7% compared to 1.4% for the HNC-STLS, see Table II.

Discussion. We have performed specially designed MD simulations to indirectly extract the bridge functions of classical OCP liquids. Systematic extractions with quantified uncertainties for 18 OCP states allowed an accurate parametrization of OCP bridge functions, which was embedded in the recently developed IEMHNC integral equation theory approach for classical YOCP liquids and in a novel IET-STLS dielectric scheme for quantum OCP liquids. To enable benchmarking, extensive PIMC simulations for 14 quantum OCP liquid states were also carried out. For both liquids, the structural and thermodynamic

properties were predicted with unprecedented precision.

Classical OCP bridge functions can also be used to explore the limits of other existing theoretical approaches. For the classical YOCP, the OCP liquid can be utilized as the reference system of the VMHNC approach instead of the Percus-Yevick hard-sphere liquid with the effective coupling determined by minimizing an approximate free energy functional [65]. For the quantum OCP, classical OCP bridge functions can be used in advanced quantum-classical mapping approaches in place of hard-sphere bridge functions [66]. Finally, although this work is dedicated to 3D one-component systems, the bridge function extraction technique, IEMHNC approach and IET-STLS scheme can be extended to 2D or multi-component cases.

Acknowledgments. This work was partly funded by the Swedish National Space Agency under grant no. 143/16. This work was also partly funded by the Center of Advanced Systems Understanding (CASUS) that is financed by Germany's Federal Ministry of Education and Research (BMBF) and the Saxon Ministry for Science, Culture and Tourism (SMWK) with tax funds on the basis of the budget approved by the Saxon State Parliament. The MD simulations were carried out on resources provided by the Swedish National Infrastructure for Computing (SNIC) at the NSC (Linköping University) that is partially funded by the Swedish Research Council under grant agreement no. 2018-05973. The PIMC simulations were carried out at the Norddeutscher Verbund für Hoch- und Höchstleistungsrechnen (HLRN) under grant no. shp00026 and on a Bull Cluster at the Center for Information Services and High Performance Computing (ZIH) at Technische Universität Dresden.

-
- [1] B. A. Remington, R. P. Drake and D. D. Ryutov, *Rev. Mod. Phys.* **78**, 755 (2006).
 - [2] V. E. Fortov, *Phys. Usp.* **52**, 615 (2009).
 - [3] G. E. Morfill and A. V. Ivlev, *Rev. Mod. Phys.* **81**, 1353 (2009).
 - [4] M. Chaudhuri, A. V. Ivlev, S. A. Khrapak, H. M. Thomas and G. E. Morfill, *Soft Matter* **7**, 1287 (2011).
 - [5] S. D. Bergeson, S. D. Baalrud, C. L. Ellison, E. Grant, F. R. Graziani, T. C. Killian, M. S. Murillo, J. L. Roberts, and L. G. Stanton, *Phys. Plasmas* **26**, 100501 (2019).
 - [6] M. Baus and J.-P. Hansen, *Phys. Rep.* **59**, 1 (1980).
 - [7] S. Ichimaru, *Rev. Mod. Phys.* **65**, 255 (1993).
 - [8] T. Dornheim, S. Groth and M. Bonitz, *Phys. Rep.* **744**, 1 (2018).
 - [9] V. Fortov, A. Ivlev, S. Khrapak, A. Khrapak and G. Morfill, *Phys. Rep.* **421**, 1 (2005).
 - [10] M. Lyon and S. L. Rolston, *Rep. Prog. Phys.* **80**, 017001 (2017).
 - [11] J. A. Barker and D. Henderson, *Rev. Mod. Phys.* **48**, 587 (1976).
 - [12] K. Trachenko and V. V. Brazhkin, *Rep. Prog. Phys.* **79**, 016502 (2016).
 - [13] K. I. Golden and G. J. Kalman, *Phys. Plasmas* **7**, 14 (2000).
 - [14] A. Diaw and M. S. Murillo, *Phys. Rev. E* **92**, 013107 (2015).
 - [15] Y. Tanada, *Phys. Rev. B* **94**, 245106 (2016).
 - [16] Yu. Arkhipov, A. Askaruly, A. Davletov, D. Dubovtsev, Z. Donko, P. Hartmann, I. Korolov, L. Conde and I. Tkachenko, *Phys. Rev. Lett.* **119**, 045001 (2017).
 - [17] B. Scheiner and S. D. Baalrud, *Phys. Rev. E* **100**, 043206 (2019).
 - [18] J. Talbot, J. L. Lebowitz, E. M. Waisman, D. Levesque and J.-J. Weis, *J. Chem. Phys.* **85**, 2187 (1986).
 - [19] J. P. Hansen and I. R. McDonald, *Theory of Simple Liquids*, (Academic Press, London, 2006).
 - [20] A. Santos, *A Concise Course on the Theory of Classical Liquids*, (Springer, Heidelberg, 2016).
 - [21] H. L. Frisch and J. L. Lebowitz, *The Equilibrium Theory of Classical Fluids*, (Benjamin, New York, 1964).
 - [22] P. Attard and G. N. Patey, *J. Chem. Phys.* **92**, 4970 (1990).
 - [23] J. Kolafa, S. Labik and A. Malijevsky, *Mol. Phys.* **100**, 2629 (2002).
 - [24] R. Fantoni and G. Pastore, *J. Chem. Phys.* **120**, 10681 (2004).
 - [25] L. Belloni, *J. Chem. Phys.* **147**, 164121 (2017).
 - [26] F. Lucco Castello, P. Tolias and J. C. Dyre, *J. Chem. Phys.* **154**, 034501 (2021).
 - [27] J. M. Bomont, *Adv. Chem. Phys.* **139**, 1 (2008).

- [28] P. Tolias and F. Lucco Castello, *Phys. Plasmas* **26**, 043703 (2019).
- [29] P. Hopkins, A. J. Archer and R. Evans, *Phys. Rev. E* **71**, 027401 (2005).
- [30] S. Hamaguchi, R. T. Farouki and D. H. E. Dubin, *Phys. Rev. E* **56**, 4671 (1997).
- [31] P. D. Poll, N. W. Ashcroft and H. E. DeWitt, *Phys. Rev. A* **37**, 1672 (1988).
- [32] G. Dharuman, L. G. Stanton, J. N. Glosli and M. S. Murillo, *J. Chem. Phys.* **146**, 024112 (2017).
- [33] J. L. Lebowitz and J. K. Percus, *Phys. Rev.* **122**, 1675 (1961).
- [34] M. Llano-Restrepo and W. G. Chapman, *J. Chem. Phys.* **97**, 2046 (1992).
- [35] S. Ogata, *Phys. Rev. E* **53**, 1094 (1996).
- [36] B. Widom, *J. Chem. Phys.* **39**, 2808 (1963).
- [37] P. Tolias, S. Ratynskaia and U. de Angelis, *Phys. Rev. E* **90**, 053101 (2014).
- [38] H. Iyetomi, S. Ogata and S. Ichimaru, *Phys. Rev. A* **46**, 1051 (1992).
- [39] B. Jancovici, *J. Stat. Phys.* **17**, 357 (1977).
- [40] M. Bonitz, C. Henning and D. Block, *Rep. Prog. Phys.* **73**, 066501 (2010).
- [41] A. A. Veldhorst, T. B. Schröder and J. C. Dyre, *Phys. Plasmas* **22**, 073705 (2015).
- [42] T. B. Schröder and J. C. Dyre, *J. Chem. Phys.* **141**, 204502 (2014).
- [43] J. C. Dyre, *J. Phys.: Condens. Matter* **28**, 323001 (2016).
- [44] U. R. Pedersen, L. Costigliola, N. P. Bailey, T. B. Schröder and J. C. Dyre, *Nat. Commun.* **7**, 12386 (2016).
- [45] O. Vaulina, S. Khrapak and G. Morfill, *Phys. Rev. E* **66**, 016404 (2002).
- [46] F. Lucco Castello and P. Tolias, *Contrib. Plasma Phys.* **61**, e202000105 (2021).
- [47] Y. Rosenfeld, *J. Stat. Phys.* **42**, 437 (1986).
- [48] R. T. Farouki and S. Hamaguchi, *J. Chem. Phys.* **101**, 9885 (1994).
- [49] T. Ott and M. Bonitz, *Contrib. Plasma Phys.* **55**, 243 (2015).
- [50] M. Bonitz, T. Dornheim, Zh. A. Moldabekov, S. Zhang, P. Hamann, H. Kählert, A. Filinov, K. Ramakrishna and J. Vorberger, *Phys. Plasmas* **27**, 042710 (2020).
- [51] F. Graziani, M. P. Desjarlais, R. Redmer and S. B. Trickey, *Frontiers and Challenges in Warm Dense Matter*, (Springer International, Switzerland, 2014).
- [52] E. Wigner, *Phys. Rev.* **46**, 1002 (1934).
- [53] N. D. Drummond, Z. Radnai, J. R. Trail, M. D. Towler and R. J. Needs, *Phys. Rev. B* **69**, 085116 (2004).
- [54] S. Ichimaru, *Statistical Plasma Physics Vols. I & II* (CRC Press, Boca Raton, 2018).
- [55] S. Tanaka and S. Ichimaru, *J. Phys. Soc. Jpn.* **55**, 2278 (1986).
- [56] K. S. Singwi, M. P. Tosi, R. H. Land and A. Sjölander, *Phys. Rev* **176**, 589 (1968).
- [57] S. Ichimaru, H. Iyetomi and S. Tanaka, *Phys. Rep.* **149**, 91 (1987).
- [58] T. Dornheim, A. Cangi, K. Ramakrishna, M. Böhme, S. Tanaka and J. Vorberger, *Phys. Rev. Lett.* **125**, 235001 (2020).
- [59] T. Dornheim, Z. A. Moldabekov and P. Tolias, *Phys. Rev. B* **103**, 165102 (2021).
- [60] S. Tanaka, *J. Chem. Phys.* **145**, 214104 (2016).
- [61] T. Dornheim, T. Sjostrom, S. Tanaka and J. Vorberger, *Phys. Rev. B* **101**, 045129 (2020).
- [62] K.-C. Ng, *J. Chem. Phys.* **61**, 2680 (1974).
- [63] F. Lucco Castello and P. Tolias, *Phys. Rev. E* **103**, 063205 (2021).
- [64] T. Dornheim, *Phys. Rev. E* **100**, 023307 (2019).
- [65] F. Lado, S. M. Foiles and N. W. Ashcroft, *Phys. Rev. A* **28**, 2374 (1983).
- [66] Y. Liu and J. Wu, *J. Chem. Phys.* **140**, 084103 (2014).